Dynamics controlled by magnetic fields: parallel astrophysical computations

R. Keppens

keppens@rijnh.nl, FOM-Institute for Plasma Physics 'Rijnhuizen',
P.O. Box 1207, 3430 BE Nieuwegein, The Netherlands*

I present the development history of and the obtained flexibility within the Versatile Advection Code [VAC, see http://www.phys.uu.nl/~toth], a software package for solving sets of – near – conservation laws in any dimensionality. Using a finite volume discretization on a static structured grid, the versatility resides in the choice of applications (Euler, Navier-Stokes, Magneto-Hydro-Dynamics), geometry, computer platform, shock-capturing spatial and temporal discretizations. For distributed memory execution, the VAC source code is automatically preprocessed to High Performance Fortran which results in fully scalable applications.

In its most challenging configuration, the code is used for simulating magnetized plasma dynamics in astrophysically relevant, three-dimensional geometries. The magnetic field can severely complicate plasma flow behaviour both in shock-dominated and otherwise (un)steady regimes. We present examples of (i) 'kinking' magnetic flux tubes, related to emerging sunspots on the solar surface; (ii) Kelvin-Helmholtz unstable magnetized jet flows, present at all scales in our universe; and (iii) coronal mass ejections in the continuously expanding solar magnetic environment. All these simulations would benefit greatly from dynamically controlled grid adaptivity, a research topic we are currently investigating.

1. VERSATILE ADVECTION CODE

1.1. Motivation: Astro-Plasma-Physics

Highly ionized plasma dynamics is encountered in virtually all astrophysical phenomena. In many of these, magnetic fields play a crucial role. Perhaps the best known examples are found throughout the solar atmosphere, where magnetic activity is at play in sunspots on the solar surface, in the intricate loop-like structuring of the solar corona, and throughout the entire solar heliosphere where the solar wind interacts with planetary magnetospheres. Particularly violent events are the coronal mass ejections, when

*Work done within the association agreement of Euratom and the 'Stichting voor Fundamenteel Onderzoek der Materie' (FOM) with financial support from the 'Nederlandse Organisatie voor Wetenschappelijk Onderzoek' (NWO) and Euratom. It is part of a project on 'Parallel Computational Magneto-Fluid Dynamics', an NWO Priority Program on Massively Parallel Computing. Use of computing facilities is funded by 'Nationale Computer Faciliteiten' (NCF). I thank G. Tóth, J.P. Goedbloed, A.J.C. Beliën, R.B. Dahlburg, P.A. Zegeling, M. Nool for fruitful collaborations.

destabilized magnetic field complexes erupt and lead to global disturbances of the solar environment. From a plasma physical viewpoint, these processes involve a wealth of linear and nonlinear wave dynamics, with bow shocks, current sheets, flux tubes, jet-like flows, as reoccuring basic concepts. Computational Magneto-Fluid Dynamics (CMFD) is rapidly evolving into the prime means to advance our understanding of such complex magnetized plasma behavior. The Versatile Advection Code was developed in a collaborative effort on parallel CMFD.

1.2. Philosophy and Discretizations

The Versatile Advection Code (VAC) was designed from the start [1] to solve systems of conservation laws in 1, 2, or 3-dimensional settings. A modular structuring of the code groups code into segments which are specific to I/O, to e.g. hydrodynamic (HD) or magnetohydrodynamic (MHD) equations, or to purely grid or discretization related matters. The code employs a finite volume discretization on a structured grid, and the dimensionality is unspecified in the source code through the use of the Loop Annotation SYntax (LASY) [2]. Using Perl scripts, the LASY-augmented Fortran 90 code can be preprocessed to Fortran 77, Fortran 90, or High Performance Fortran, making VAC easily portable between all UNIX-based platforms [3]. The code is available via registration on `http://www.phys.uu.nl/~toth`, where regularly updated publication lists document the progress. An extensive user manual, complete with examples of VAC usage, can also be found there.

Shock-capturing discretizations implemented [4] include variants of the Flux Corrected Transport type [5] and several Total Variation Diminishing (TVD) schemes [6]. The MHD simulations reported below make use of the one step TVD scheme with a Roe-type approximate Riemann solver [7], or of the robust and simple predictor-corrector TVD-Lax Friedrich (TVDLF) method [8] which just uses the fastest wave speed in the numerical flux definition. All problems advance the MHD equations explicitly in time, while there are options provided in VAC for problem-specific choices of semi-implicit and fully implicit time integration strategies [9,10]. The finite volume discretization with cell-centered variables lends itself naturally to the specification of boundary conditions through the use of ghost cells.

1.3. The Magnetohydrodynamic Module

For simulating magnetically controlled plasma flow, one selects the set of partial differential equations corresponding to one-fluid MHD:

$$\frac{\partial \rho}{\partial t} + \nabla \cdot (\mathbf{v}\rho) = S_\rho \tag{1}$$

$$\frac{\partial \rho \mathbf{v}}{\partial t} + \nabla \cdot (\mathbf{v}\rho\mathbf{v} - \mathbf{B}\mathbf{B}) + \nabla(p + \mathbf{B}^2/2) = \vec{S}_{\rho v} \tag{2}$$

$$\frac{\partial e}{\partial t} + \nabla \cdot \Big(\mathbf{v}e + \mathbf{v}(p + \mathbf{B}^2/2) - \mathbf{B}\mathbf{B}\cdot\mathbf{v}\Big) = S_e \tag{3}$$

$$\frac{\partial \mathbf{B}}{\partial t} + \nabla \cdot (\mathbf{v}\mathbf{B} - \mathbf{B}\mathbf{v}) = \vec{S}_B, \tag{4}$$

so that in 3D problems, the eight unknowns represent the density ρ, the components of the momentum vector $\rho\mathbf{v}$, the total energy density e, and the vector magnetic field $\mathbf{B}$.

Sources and sinks are collected in the right-hand-side terms, representing e.g. Ohmic losses through resistivity. These terms vanish for ideal MHD problems. The primitive pressure variable p is related to the energy density through $p = (\gamma - 1)(e - \rho \mathbf{v}^2/2 - \mathbf{B}^2/2)$ with adiabatic index γ. In the examples that follow, we take $\gamma = 5/3$ if not stated otherwise. Units of $\mathbf{B}$ are chosen such that the magnetic permeability is unity and this field must further obey the law $\nabla \cdot \mathbf{B} = 0$. This latter property poses a non-trivial complication for modern shock-capturing schemes, and a recent, thorough evaluation of seven different ways of ensuring it in multi-dimensional MHD simulations with VAC is found in [11]. We typically took a projection scheme approach [12] or followed Powell's eight-wave formulation [13].

2. COMPUTATIONAL MAGNETO-FLUID DYNAMICS

At first sight, the ideal MHD equations provide a straightforward extension of the Euler system: a Lorentz force appears as an additional means to transfer momentum, and the extra vector variable $\mathbf{B}$ obeys yet another conservation law. However, the dynamical influence of the magnetic field $\mathbf{B}$, its interwoven character with the flow field $\mathbf{v}$ through the induction equation, and the topological constraint arising from $\nabla \cdot \mathbf{B} = 0$, can lead to significant alterations of simplified flow problems. Physically, these complications are due to the presence of 7 wave speeds, instead of the 3 speeds $[v - c_s, v, v + c_s]$ dealt with in compressible hydrodynamic cases with sound speed c_s. In MHD, entropy disturbances still travel with the flow speed v, but there are now three pairs of co- and counter travelling slow magnetosonic, magnetic Alfvén, and fast magnetosonic wave signals. These waves are anisotropic: localized perturbations influence directions along and across the magnetic field differently.

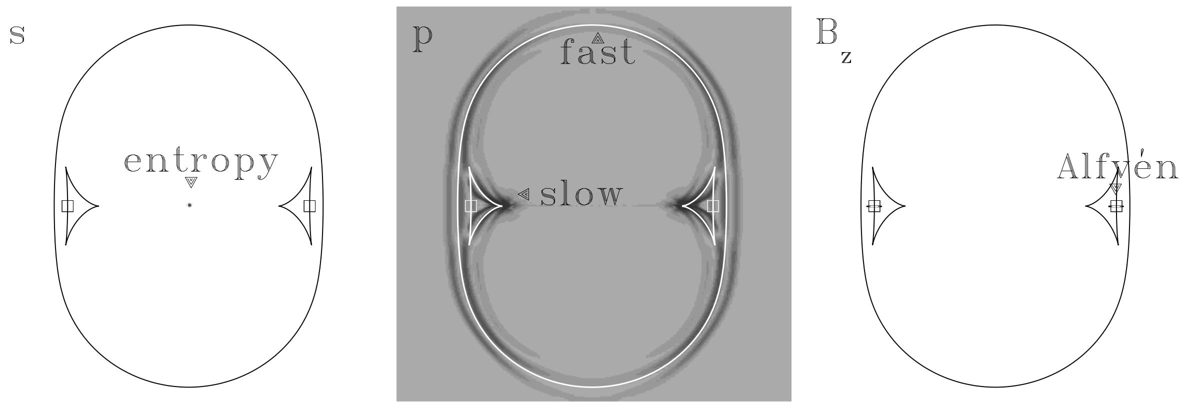

Figure 1. A 2.5D MHD simulation of a localized p, ρ, and v_z perturbation in a static, homogeneous plasma generates numerically the – overplotted – theoretical Friedrichs diagram. The background state has a horizontal magnetic field and is characterized by the ratio $c_s/v_A = 1.11$. Plotted are the entropy $s = p\rho^{-\gamma}$ [left], the thermal pressure p [middle], and the transverse component of the magnetic field B_z [right], at a finite time after the imposed perturbation. The different wave signals are labeled according to type. Note the extreme anisotropy between field-aligned and cross-field directions.

Figure 1 shows a VAC simulation result of impulsively generated MHD waves in a static, homogeneous, magnetized plasma. Taking $\rho = 1$, $p = 0.6$ and $\mathbf{B} = 0.9\hat{\mathbf{e}}_x$, a localized 10 % perturbation in density and pressure, together with a co-spatial velocity pulse $\mathbf{v} = 0.01\hat{\mathbf{e}}_z$ perpendicular to the simulated (x, y)-domain, triggers all MHD wave modes. In particular, the almost pointwise velocity pulse results in two transverse, similarly pointwise Alfvén waves that are only seen in the transverse B_z and v_z components. They are purely magnetically driven and travel only along the (horizontal) fieldlines at the characteristic Alfvén speed $v_A = B/\sqrt{\rho}$. For the time shown, these Alfvén signals are at the location of the squares in the diagram. The pressure field contains slow and fast wave signals, with anisotropic wavefronts. For a pure pointlike perturbation, the wavefronts are given by the theoretical Friedrichs diagram, which is overplotted in each frame. Note how the polarization of the individual wave signals are fully obeyed: there is no entropy or transverse B_z variation associated with the latter two waves. An entropy discontinuity is only seen at the origin, where the pulse was imposed in the static medium.

2.1. Steady and unsteady shock-dominated simulations

Ultimately, the different linear MHD wave modes can lead to complicated shock patterns in the ensuing nonlinear dynamics. Different shock types are distinguished when upstream and downstream states connect *super-* to *sub-* fast, Alfvén, and slow flow regimes. A *fast magnetosonic shock* keeps the flow super-Alfvénic but goes from super-fast upstream to sub-fast downstream. An *intermediate shock* occurs when the Alfvén speed is crossed, while a *slow shock* involves a jump across the slow magnetosonic speed. Depending on the relative importance of magnetic, thermal and kinetic energies, as e.g. characterized by the plasma beta $\beta = 2p/B^2$ and the Alfvén Mach number $M_A = v/v_A$, one distinguishes between magnetically dominated, pressure-dominated, or flow-dominated scenarios.

An intrinsic magnetically dominated effect was recently investigated by De Sterck *et al.* [14]. They analysed up-down symmetric bow shocks occuring when 2D, field-aligned, super-fast flow impinges on a perfectly conducting cylindrical obstacle. For upstream states in the *switch-on* regime, with $\beta < 2/\gamma$ and

$$1 < M_A < \sqrt{\frac{\gamma(1-\beta)+1}{\gamma-1}},$$

the bow shock contains several shock segments of different type. The shock front becomes concave-outward about the symmetry stagnation line, in sharp contrast with the more familiar case from hydrodynamic simulations, where a single concave-inward bow shock forms. This can have implications for magnetospheric bow shocks and for shock structures induced by coronal mass ejections. Figure 2 shows the magnetic field lines, together with the density pattern in a greyscale contour plot, for magnetically dominated upstream conditions as in [14], namely $\beta = 0.4$ and $M_A = 1.5$. The calculation was done with VAC on an elliptical, stretched grid of size 120^2. The figure zooms in on the interacting shock segments in front of the obstacle. For an extensive analysis of the elliptic and hyperbolic flow regions present, we refer to [15]. Two-dimensional, pressure-dominated, single MHD bow shock flows, as well as the $\mathbf{B}$-dominated, multiple-shock scenarios from Figure 2, served to demonstrate in [9,10] the obtainable computational efficiency when using a fully implicit time integration scheme, instead of explicit time marching towards steady-state. These implicit calculations used Courant numbers of 100 up to 1000.

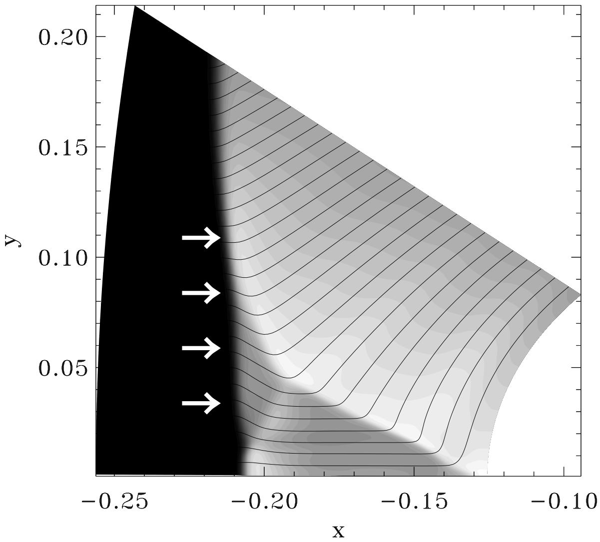

Figure 2. A magnetically dominated super-fast flow (arrows) upstream of a perfectly conducting cylindrical obstacle (bottom right) results in a steady bow shock consisting of multiple interacting shock segments. We show the density in greyscale and the magnetic fieldlines.

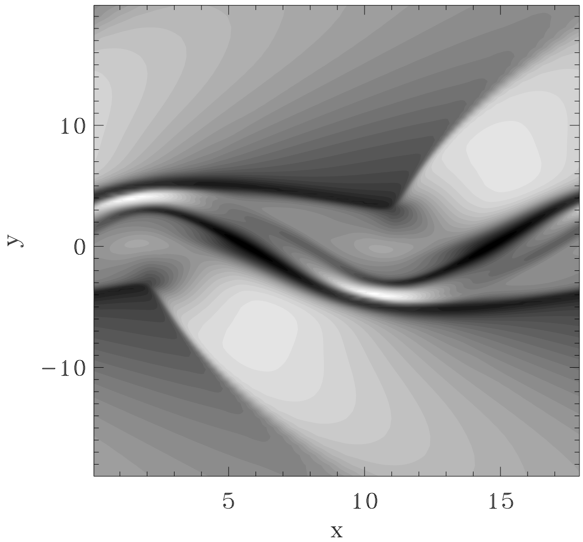

Figure 3. An unsteady magnetized wake can develop significant density variations due to sinuous instabilities. This snapshot of the density structure in the evolution of a supersonic, super-Alfvénic wake clearly reveals the presence of fast magnetosonic shocks above and below the wake.

Figure 3 contrasts the steady, magnetically dominated case from Figure 2 with a snapshot of an unsteady, flow-dominated simulation. Shown is the density structure in a section of an evolving magnetized wake [16], which must be periodically repeated along the streamwise x-direction. Originally, the wake configuration was given by a planar velocity profile $\mathbf{v} = [1 - \mathrm{sech}(y)]\hat{\mathbf{e}}_x$ which models a low speed 'wake' sandwiched between high speed flow regimes. A 3D, sheared magnetic field of constant magnitude pervades the wake, with components given by $B_x = A\ \tanh(y),\ \ B_z = A\ \mathrm{sech}(y)$. The field rotates about the y-axis from parallel alignment with the flow in the upper $y \gg 0$ regions, becomes perpendicular to the flow plane at $y = 0$, and is antiparallel to $\mathbf{v}$ in $y \ll 0$. We start with uniform density and pressure throughout – taking $\rho = 1$ and $p = 1/\gamma M^2$ – and consider a supersonic $M = 3$, super-Alfvénic $M_A = 1/A = 5$ case. A linear stability analysis – as in [17] – of this shear-flow, sheared-$\mathbf{B}$ system reveals that it is unstable to kink-like, transverse (y-direction) displacements. At the time shown, this sinuous instability has, after a period of exponential growth, led to the formation of rightwardly traveling, fast magnetosonic shocks both above and below the transversely swaying wake. The grid employed is a 200×200 vertically stretched Cartesian mesh. With a plasma beta $\beta = 3.33$, this configuration could serve to mimick conditions far out in the heliospheric current sheet, where the slow solar wind is found in between fast wind regions. It will be of interest to consider 3D scenarios where the background 'wake' flow accelerates from sub- to super-Alfvénic wind. In what follows, we give examples of 3D MHD studies which highlight the role of the magnetic field in fully nonlinear plasma dynamics.

2.2. Knotting a flux tube

This first example illustrates that the magnetic Lorentz force contains two potentially opposing contributions: it can be decomposed in an isotropic magnetic pressure $-\nabla\frac{B^2}{2}$ and a tension part $(\mathbf{B}\cdot\nabla)\mathbf{B}$ along the field lines. As a result, magnetized plasma gets accelerated from high to low magnetic field strength regions and curved field lines have a tendency towards straigthening. When one then considers an isolated magnetic flux tube with *twisted* field lines, the axial $\mathbf{B}$-component tries to prevent helical deformations through tensional forces, while the azimuthal component B_φ acts destabilizing through the magnetic pressure. Therefore, a flux tube is *kink-unstable* when a critical twist $q = B_\varphi/rB_z > q_{crit}$ is exceeded.

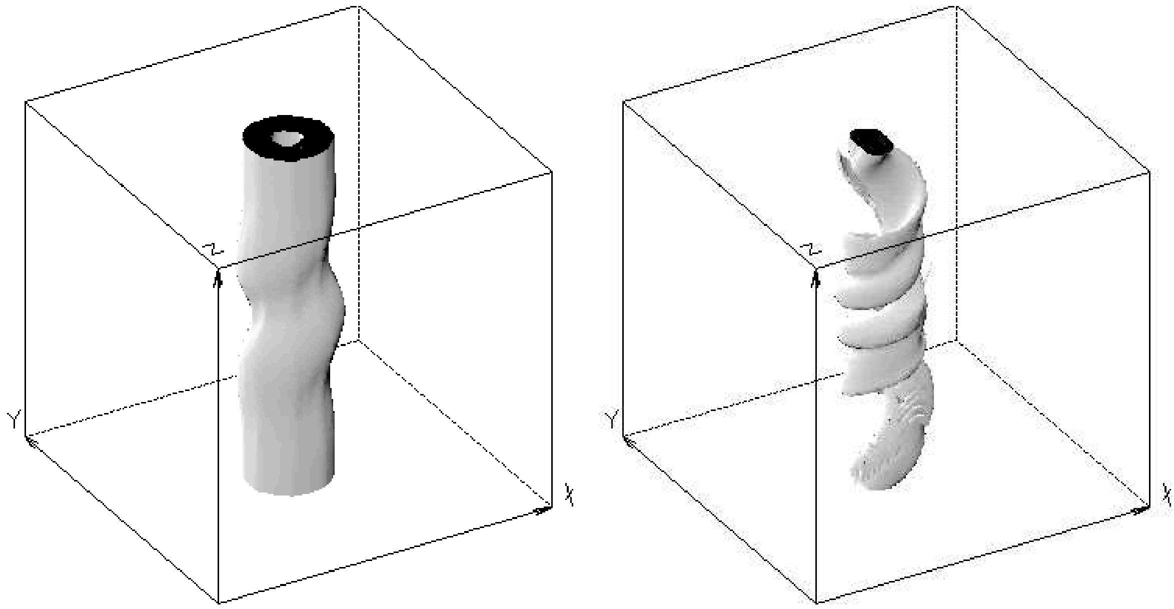

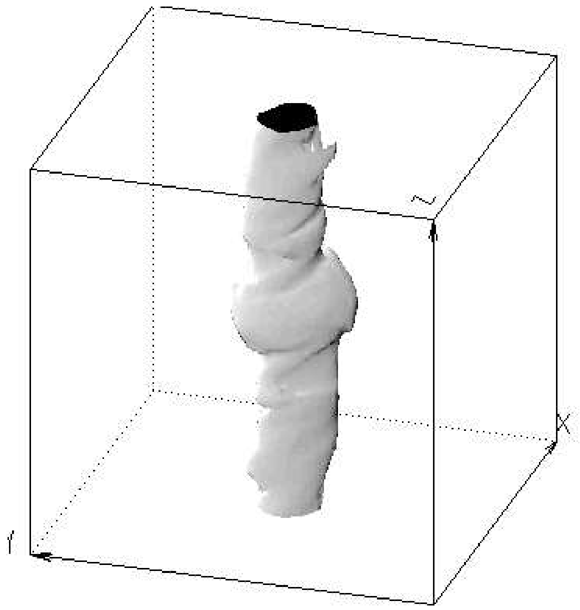

Figure 4. The evolution of a kink unstable flux tube as seen in isosurfaces of the magnetic field strength. Top row: a helical deformation self-amplifies. Kink instabilities of varying axial wavelength interact. Shown are isosurfaces of the instantaneous $\mid \mathbf{B} \mid_{max}/2$ at times $t = 2.5$ and $t = 3.5$. At right: constructive interference leads to the formation of a central 'knot', shown at time $t = 10$ as the isosurface $\mid \mathbf{B} \mid_{max}/3$.

Linton *et al.* [18] performed detailed numerical studies of such kink-unstable flux tubes using a 3D spectral code. The aim was to assess whether the complex magnetic field structure observed in so-called δ-sunspots could be related to this fundamentally magnetic instability. With VAC, we could recover their most striking result, namely that the nonlinear, constructive interference of several unstable, linear kink modes can lead to the formation of a concentrated 'knot'. The simulation considers a flux tube with an aspect ratio given by $R/L = 1/8$ and of constant normalized twist $\bar{q} \equiv qR = 5.98$ embedded in unmagnetized, uniform surroundings. Setting the axial field component to $B_z = (1 - r^2/R^2)^{1/4}$, the density to $\rho = 1$, and the pressure profile within the tube according to

$$p(r < R) = \frac{1}{2}\left(\beta_o + 1 - \frac{2\bar{q}^2}{3}\right) - \sqrt{1 - \frac{r^2}{R^2}}\left(\frac{1}{2} - \frac{\bar{q}^2}{3} + \frac{5\bar{q}^2}{6}\frac{r^2}{R^2}\right),$$

one can impose the value for the axial plasma beta β_o. Taking $\beta_o = 600$, it was argued that the physical conditions for flux tubes stored at the base of the solar convection zone were closely met. As the twist significantly exceeds the critical twist of $q_{crit}R = 0.5$, the tube is unstable to kink instabilities of varying axial wavelength. Instead of perturbing the tube with the exact linear kink eigenfunctions as done in [18], our simulation simply induced multi-mode kinks by applying a purely radial velocity perturbation given by

$$v_r = \delta v_r e^{-\left(\frac{r/R-1}{\sigma}\right)^2} \sum_{n=1}^{n=7} \frac{L/R}{2\pi n} \cos\left(\varphi - 2\pi n \frac{z}{L}\right).$$

We used a 100^3 Cartesian grid and took $\sigma = 0.2$ and $\delta v_r = 0.01$. Figure 4 shows isosurfaces of magnetic field strength at 2.5, 3.5, and 10 units of the Alfvén crossing time R/v_A. The first two frames clearly show the initial helical deformation and the appearance and interaction of several 'kinks'. The final frame depicts the 'knotted' structure that develops. When analyzing the magnetic field structure throughout this concentrated kink, Linton *et al.* found a striking similarity with δ-sunspot fields. Using the flexibility of VAC for adding gravitational source terms and switching from triple-periodic (as done for the spectral calculations) to boundary conditions consistent with a background stratification, it is the intention to simulate the development of these kinking flux tubes *as they rise through the solar convection zone.* This will make an explicit connection between kink-unstable flux tubes in the solar interior and complex δ-spot emergence observed on the solar surface.

2.3. Disrupting jets

Our second example serves to show that even in those circumstances where the magnetic field is weak initially and can thus safely be ignored for predicting the *linear stability* of stationary plasma equilibria, the *nonlinear evolution* can become magnetically controlled. This was demonstrated in [19], where Kelvin-Helmholtz unstable jets were investigated. The Kelvin-Helmholtz instability – well-known from wind-induced waves on the surface of a pond – is in essence a hydrodynamical instability occuring at the interface between fluids that move at different speeds. Considering a cylindrical jet flow with

$$\mathbf{v} = V_o \tanh \frac{r - R_{jet}}{0.1 R_{jet}} \hat{\mathbf{e}}_x,$$

in a uniform magnetic field $\mathbf{B} = B_o\hat{\mathbf{e}}_x$, 3D MHD simulations allow to address the role of compressibility and magnetic forces when the shear flow about $r = R_{jet}$ is Kelvin-Helmholtz destabilized. Keppens & Tóth [19] analyzed cases where the characterizing dimensionless parameters typified a pressure and flow-dominated situation with $\beta = 120$, $M_A = 5$, for a subsonic $M = 0.5$ jet with aspect ratio $R_{jet}/L = 1/2$. An analytic treatment of the quasi-linear regime neglected the influence of magnetic fields altogether and could correctly predict the first-excited couplings between linear (m, n) modes with variations $\cos(m\varphi)\sin(n2\pi z/L)$. However, in the further evolution, it was demonstrated that the magnetic field becomes locally amplified and influences the jet deformation dynamically.

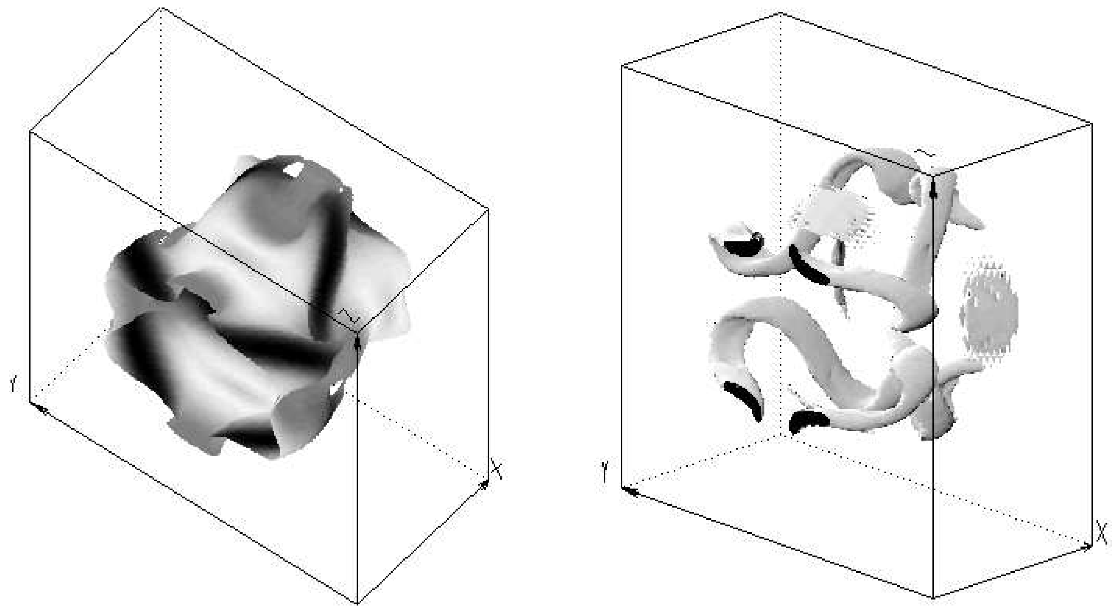

Figure 5. A Kelvin-Helmholtz unstable cylindrical jet deforms in a manner which is additionally regulated by locally amplified magnetic fields. Well within the nonlinear evolution, we show the jet surface shaded by thermal pressure at left. Note the fibril strands of dark, low pressure zones. These are cospatial with concentrated magnetic fields: the right panel shows isosurfaces where $\log_{10}(B_r^2 + B_\varphi^2) = -1.36$.

Figure 5 is generated by a 3D $50 \times 100 \times 100$ simulation of an unstable, magnetized jet. It shows the jet surface where v_x vanishes, shaded by the thermal pressure variation. Instead of an induced $(m, n) = (1, 1)$ excitation as was used for Figure 3 in [19], we perturbed the jet with a $(2, 1)$ radial velocity. The time depicted corresponds to four times the isothermal sound crossing time $L/\sqrt{p/\rho}$ within which the pressure has changed from uniform throughout to become $m = 4$ modulated about the jet circumference. Four low pressure, dark strands can be distinguished and they coincide with loci of amplified magnetic fields. This is demonstrated in the right panel showing an isosurface of strong poloidal fields. Besides four fibril-like concentrations of the magnetic field, one can distinguish four sheet-type structures which intersect high-pressure, high-density compression zones. These latter structures are reminiscent of what had previously been studied in initially uniformly magnetized, 2D shear flows [20]. Locally, Lorentz forces can no longer be ignored and the **B** field plays a prominent role in the further shaping and breakup of the jet flow. Future work can address the role of magnetic shear cospatial with the jet surface, as was done in two-dimensional resistive MHD simulations where reconnection events were triggered [20].

2.4. Solar mass ejections

Our final example of magnetized plasma dynamics relates to the global magnetic reconfigurations of the solar heliosphere associated with coronal mass ejections. These almost daily, violent mass loss events can potentially influence the earth's magnetosphere, making their study of central importance for *space weather* predictions. They occur within the continuously expanding solar corona, combining the intricacies of stationary transonic solar wind modeling [21,22] with highly time-varying dynamics.

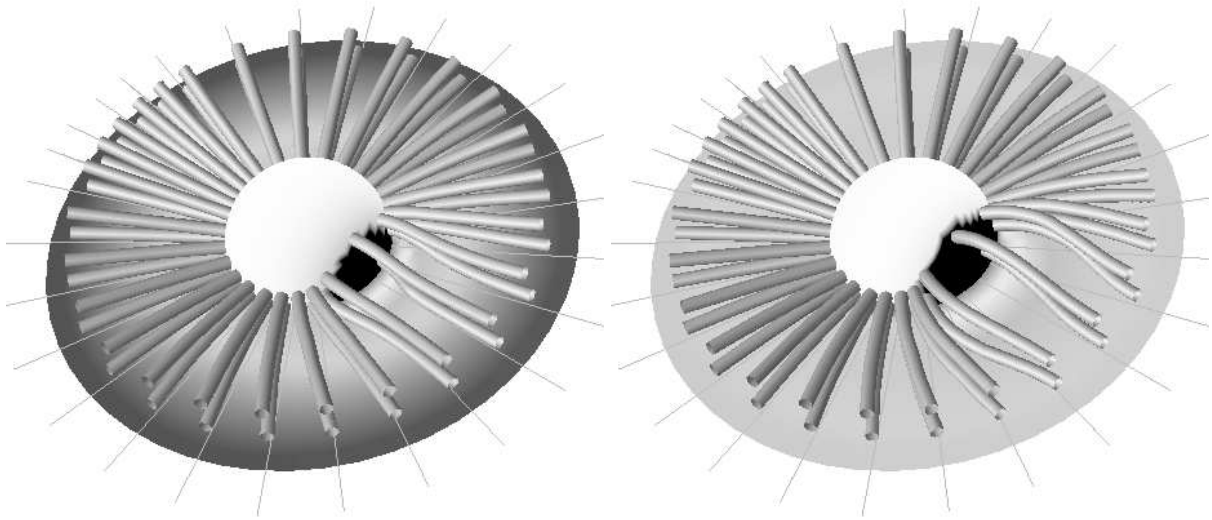

Figure 6. An analytic, 3D time-dependent MHD solution for a self-similarly expanding coronal mass ejection in the magnetized solar wind is recovered numerically. Looking down on the pole, the solar surface is shaded by the magnitude of the magnetic field: the black area marks the protrusion of the expanding bubble. Several field lines are drawn as tubular structures. The equatorial plane is shaded according to the density stratification. Two consecutive times show the CME expansion.

As a stepping stone towards ambitious realistic modeling, we first set forth to recover numerically an analytical, 3D time-dependent MHD solution by Gibson & Low [23] mimicking a coronal mass ejection. The formidable task of getting a closed form solution to the full set of MHD equations was achieved in [23] through a sequence of mathematical transformations. The first one involved getting rid of the explicit time dependence through a self-similar transformation to the variable $\zeta \propto r/t$ and assuming a purely radial outflow $\mathbf{v} = (r/t)\hat{\mathbf{e}}_r$. Starting from spherical coordinates (r, θ, φ), this reduces the set of MHD equations to a 3D 'magnetostatic' problem in (ζ, θ, φ) variables. The second realization from Gibson & Low was that the geometric stretching procedure $r \to r - a$ can relate different magnetostatic solutions in a straightforward manner. It also contracts an off-origin sphere σ into a tear-shaped 'bubble'. Hence, the combined transformations would result in an analytic solution for a self-similarly expanding bubble-shaped coronal mass ejection in the solar wind, when one can solve for a magnetostatic atmosphere both inside and outside an off-center sphere. The published model combined a potential $\mathbf{B}$ solution (with $\nabla \times \mathbf{B} = 0$) outside the sphere σ with an axisymmetric 'spheromak' $\mathbf{B}$ field configuration inside σ. The geometrical stretching breaks the axisymmetry of the internal field, resulting in a truly 3D time-dependent solution. The only extra complication is to perform a matching procedure across the deformed bubble boundary that ensures the pressure balance there.

Figure 6 shows two snapshots of a fully 3D time-dependent MHD simulation on a 50^3 spherical grid which recovers the self-similar expansion known from the explicit analytic solution. Since the initial condition considered a hydrostatic solution interior to the contracted sphere σ, with the magnetized exterior constructed as in [23], this particular evolution is axisymmetric about the axis connecting the origin and the σ-centre. This preserved symmetry serves as an extra check on the obtained numerical solution. Note how the hydrostatic bubble expands as it rises through the solar surface, pushing aside the magnetic field lines in the stratified surroundings. It is our intention to recover the 3D magnetized bubble evolution as well and explore meaningful variations that are no longer tractable analytically. These could be the inclusion of solar rotation, changes in the polytropic index ($\gamma = 4/3$ for the analytic solution), or simulating the CME detachment from the coronal base. All these effects would make the expansion no longer self-similar in r/t and bring the model closer to realistic scenarios.

3. OUTLOOK

The continued development and application of the Versatile Advection Code has already brought several new insights in algorithmic as well as specific plasma physical and astrophysical issues. Computational science achievements include: (1) the possibility for doing fair comparisons between different spatial and temporal discretizations adopted for solving the same multi-dimensional HD or MHD problems [4,9–11]; (2) the invention of the original Loop Annotation SYntax for writing a CFD code independent of the dimensionality [2]; (3) the development and succesful demonstration of new numerical algorithms [11]; (4) the obtained linear speedup on shared and distributed memory parallel platforms [3]. Besides the applications already discussed, physics driven achievements comprise among others: a new assesment of the efficiency of footpoint driven, thermally stratified solar coronal loops [24]; the simulation of bi-directional jet flows precursed and bounded by different MHD shock fronts comparing favorably with several aspects known from solar microflare observations [25]; getting accurate stationary transonic stellar wind solutions for varying magnetic field strength and topology, rotation rate, etc. [22].

In the examples above, we indicated several directions for future research. A lot can be learned from simplified, but at the same time sophisticated, model problems. Ultimately, realistic models of e.g. the solar heliosphere must combine all knowledge collected from

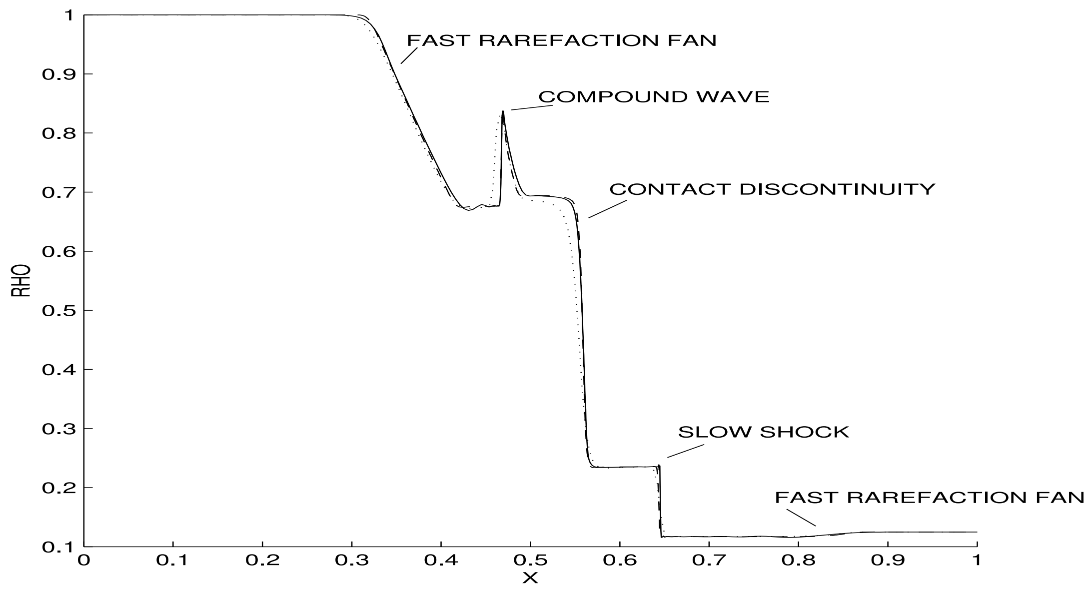

Figure 7. The density at time $t = 0.1$ for the Brio-Wu shock tube problem. Out of the initial two-state discontinuity, five nonlinear flow features develop which are named according to type. We compare a moving grid solution exploiting 250 grid points (solid line) with a solution from VAC on a static 250 grid (dotted) and on a high resolution 1000 point grid (dashed line).

idealized studies as described above: coronal loops act as waveguides for linear MHD waves, current and/or shear flow driven instabilities may reconfigure the magnetic topology locally, complex MHD shocks can be induced impulsively by coronal mass ejections or they may form as the natural outcome of instabilities associated with the heliospheric current sheet. For achieving a fair amount of realism in the numerical simulations while keeping the computational costs within reasonable limits, it is highly desirable to combine the flexibility of VAC with some means of dynamic grid adaptivity. We are presently exploring two routes [26]: (i) the use of adaptive mesh refinement [27] where hierarchically nested, subsequently finer grid patches are created and removed when needed; and (ii) the use of dynamic-regridding methods where the partial differential equations of the MHD system are coupled to adaptive grid PDEs describing the mesh movements. As an example, we show in Figure 7 a comparison of two static grid VAC solutions exploiting the one step TVD method, with one dynamically-regridded solution of a 1D magnetic shock tube problem. The description is taken from [28] and shown is the resulting density structure which spontaneously develops out of the initial Riemann data. Note how almost all nonlinear flow features appear in this very simple model problem. The adaptive method-of-line solution is clearly more accurate than the static solution employing an equal amount of grid points and achieves a resolution corresponding to a four times finer static grid. High resolution, parallel CMFD simulations, possibly exploiting solution-adaptive meshes, will certainly provide many more exciting insights in magnetically controlled plasma evolution.

REFERENCES

1. G. Tóth, Astrophys. Lett. & Comm. 34 (1996) 245.
2. G. Tóth, J. Comput. Phys. 138 (1997) 981.
3. R. Keppens and G. Tóth, Parallel Computing 26 (2000) 705.
4. G. Tóth and D. Odstrčil, J. Comput. Phys. 128 (1996) 82.
5. J.P. Boris and D.L. Book, J. Comput. Phys. 11 (1973) 38.
6. A. Harten, J. Comput. Phys. 49 (1983) 357.
7. P.L. Roe and D.S. Balsara, SIAM J. Appl. Math. 56 (1996) 57.
8. H.C. Yee, NASA TM-101088 (1989).
9. R. Keppens, G. Tóth, M.A. Botchev, and A. van der Ploeg, Int. J. for Numer. Meth. in Fluids 30 (1999) 335.
10. G. Tóth, R. Keppens, and M.A. Botchev, Astron. & Astrophys. 332 (1998) 1159.
11. G. Tóth, J. Comput. Phys. 161 (2000) 605.
12. J.U. Brackbill and D.C. Barnes, J. Comput. Phys. 35 (1980) 426.
13. K.G. Powell, ICASE Report No 94-24, Langley, VA (1994).
14. H. De Sterck, B.C. Low, and S. Poedts, Phys. of Plasmas 5 (1998) 4015.
15. H. De Sterck, B.C. Low, and S. Poedts, Phys. of Plasmas 6 (1999) 954.
16. R. Keppens, R.B. Dahlburg, and G. Einaudi, Proc. of '27th EPS conference on controlled fusion and plasma physics', Budapest, 12-16 June (2000).
17. R.B. Dahlburg and G. Einaudi, Phys. of Plasmas 7 (2000) 1356.
18. M.G. Linton, G.H. Fisher, R.B. Dahlburg, and Y. Fan, Astrophys. J. 522 (1999) 1190.
19. R. Keppens and G. Tóth, Phys. of Plasmas 6 (1999) 1461.
20. R. Keppens, G. Tóth, R.H.J. Westermann, and J.P. Goedbloed, J. Plasma Phys. 61 (1999) 1.
21. R. Keppens and J.P. Goedbloed, Astron. & Astrophys. 343 (1999) 251.
22. R. Keppens and J.P. Goedbloed, Astrophys. J. 530 (2000) 1036.
23. S.E. Gibson and B.C. Low, Astrophys. J. 493 (1998) 460.
24. A.J.C. Beliën, P.C.H. Martens, and R. Keppens, Astrophys. J. 526 (1999) 478.
25. D.E. Innes and G. Tóth, Solar Phys. 185 (1999) 127.
26. R. Keppens, M. Nool, P.A. Zegeling, and J.P. Goedbloed, Lect. Notes in Comp. Science 1823 (2000) 61.
27. M.J. Berger, SIAM J. Sci. Stat. Comput. 7 (1986) 904.
28. M. Brio and C.C. Wu, J. Comput. Phys. 75 (1988) 400.

Dynamics controlled by magnetic fields: parallel astrophysical computations

R. Keppens[1]

Invited talk at ***Parallel CFD 2000*****, Trondheim, Norway. May 22-25, 2000.**

Appeared in: *Parallel Computational Fluid Dynamics – Trends and Applications*, C.B. Jenssen et al. (eds.), 2001, Elsevier Science B.V., 31-42.

[1]`keppens@rijnh.nl`, FOM-Institute for Plasma Physics 'Rijnhuizen', P.O. Box 1207, 3430 BE Nieuwegein, The Netherlands